Synthesis, Structural Determination and Antibacterial Properties of Zinc(II) Complexes Containing 4-Aminopyridine Ligands

I Wayan Dasna[1,2*], Dewi Mariyam[1], Husni Wahyu Wijaya[1,2], Ubed Sonai Fahruddin Arrozi[1], and Sugiarto Sugiarto[3]

[1]*Department of Chemistry, Faculty of Mathematics and Natural Sciences, Universitas Negeri Malang, Jl. Semarang No. 5, Malang 65145, Indonesia*

[2]*Center of Advanced Material for Renewable Energy, Universitas Negeri Malang, Jl. Semarang No. 5, Malang 65145, Indonesia*

[3]*Department of Applied Chemistry, Graduate School of Advanced Science and Engineering, Hiroshima University, 1-4-1 Kagamiyama, Higashi-Hiroshima 7398527, Japan*

Corresponding author:

email: idasna@um.ac.id

Received: March 5, 2023
Accepted: May 30, 2023

DOI: 10.22146/ijc.82801

Abstract: *Three zinc(II) complexes containing 4-aminopyridine (4-NH_2py) [Zn(4-NH_2py)$_2$(NCS)$_2$] (**1**), [Zn(4-NH_2py)$_2$Cl$_2$] (**2**), and [Zn(4-NH_2py)$_2$(NCS)Cl] (**3**) were synthesized and characterized by FTIR and single crystal X-ray diffraction. All complexes adopt a slightly distorted tetrahedral geometry with different crystal packing. Complex **1** crystallizes in the orthorhombic Pmmn space group, complex **2** in the monoclinic C2/c space group, and complex **3** in the orthorhombic Pbca space group. Non-covalent interactions such as NC-S···H, -Cl···H, and μ-μ stacking interaction between 4-NH_2py and other ligands (NCS^- and Cl^-) are observed in the crystals packing.* In vitro, *antibacterial screening of all complexes was evaluated against two bacteria (*Escherichia coli *and* Staphylococcus aureus*). The results show that **1** has the highest antibacterial activity than **2** and **3**. This difference is due to differences in the interactions elicited by the anion ligands.*

Keywords: *zinc(II) complexes; 4-NH_2py; thiocyanato; chloro ligand; antibacterial activity*

■ INTRODUCTION

Transition metal complexes of nitrogen heterocyclic ligands, such as pyridine and its derivatives, have garnered a lot of interest due to their interesting properties, such as catalysts, developing photographic images, antimicrobial agents, and thermal reaction batteries [1]. Moreover, complexes with aminopyridine have been studied due to their potential as antibacterial agents [2-4]. Complexes with aminopyridine ligand such as poli-[Cu(NCS)$_2$(x-NH_2py)$_2$] [2], [Cd(μ-L)$_2$(NH_2py)$_2$] (L = SCN^-, dca, N_3^-) [5-7], [Mn(L)$_2$(3-NH_2py)$_2$] (L = dca, SCN^-) [5-6,8] and [Co(dca)$_2$(2-NH_2py)$_2$] [3] have shown to form a polymeric structure through bidentate ligands such as dicyanamide ion (dca), nitride ion (N_3^-) and ambidentate ligand such as SCN^-. The polymeric complexes can be obtained as long as octahedral coordination of the metal center is preserved, whereas complex compounds with tetrahedral geometry such as [Zn(NCS)$_2$(x-NH_2py)$_2$] (x = 2 and 3) [9-10], [Zn(CN)$_2$(x-NH_2py)$_2$] [11], [MCl$_2$(x-NH_2py)$_2$] (M = Zn(II), Co(II) [4,12] tend to form monomeric complexes [9,13-14]. In addition, the aminopyridine ligands prefer to act as monodentate ligands, with amino groups acting as potential H-bond donors or acceptor sites [8-9,15] Meanwhile, the bidentate anion-ligands such as thiocyanate, dicyanamide, and acetate are potential ligands to form coordination polymer. This indicates that ligands and metal ions affect the structure of aminopyridine-based complexes.

The structure of the complexes also affects their antibacterial activity. Some ligands can increase the lipophilicity of complexes. The increase in lipophilicity allows it to penetrate the lipid layer of the bacterial

membrane [16]. Functional groups on pyridines such as $-NH_2$, $-OR$, $-CN$, and $-Br$ might increase antibacterial activity through the formation of bonding with lipopolysaccharides in the cell walls and change its spatial structure [17]. Complex $[CdL^I(SCN)_2]$ showed higher antibacterial activity against *Escherichia coli* and *Bacillus subtilis* than $[CdL^II]I$ (L^I = 3,10-*C*-*meso*-3,5,7,7,10,12,14,14-octamethy1-1,4,8,11-tetraazacyclotetradeca-4,11-diene) [18]. These results show that the combination of ligands is an important factor in designing effective antimicrobial agents.

In this work, we have synthesized three complexes of zinc(II) and 4-NH_2py with different anionic ligands, i.e., $[Zn(NCS)_2(4\text{-}NH_2py)_2]$ (**1**), $[ZnCl_2(4\text{-}NH_2py)_2]$ (**2**), and $[ZnCl(NCS)(4\text{-}NH_2py)_2]$ (**3**). Thiocyanate is one of the favored substrates for lactoperoxidase (LPO)-driven catalytic reduction of hydrogen peroxide (H_2O_2) to generate hypothiocyanous acid (HOSCN), a potent antimicrobial agent and better tolerated by host tissue [19-20]. Moreover, chloride (Cl^-) is one of the substrates that can generate hypochlorite (OCl^-) in myeloperoxidase (MPO) defensive peroxidase systems [21]. Chloride in the form of salt (NaCl) also inhibits microbial growth through an osmotic process. It draws water out of the bacterial cells causing the bacterial cells to shrink and die [22-23]. Therefore, chloride and thiocyanate anions were used in this study. *In vitro*, the antibacterial activity of the three complexes was also evaluated against *Staphylococus aureus* and *Escherichia coli*.

■ EXPERIMENTAL SECTION

Materials

The materials used in this study, zinc(II) chloride anhydrous ($ZnCl_2$, Merck, p.a. 98%), potassium thiocyanate (KSCN, Emsure, p.a. 99%), 4-aminopyridine (4-NH_2py, Sigma Aldrich, p.a. 98%), methanol (CH_3OH, Emsure p.a. 99%), and aquadest, were used without further purification.

Instrumentation

The instrumentations used in this study were Fourier-transform spectrophotometer (IRPrestige21, Shimadzu, Japan), conductivity meter (Cyberscan CON 11/110, Eutech Instruments, USA), X-ray single crystal diffraction spectroscopy (Bruker SMART APEX 2, USA), and melting point apparatus (Fisher-John 48061, Thermo Scientific, USA).

Procedure

Synthesis of complex $[Zn(NCS)_2(4\text{-}NH_2py)_2]$

A $ZnCl_2$ (0.1363 g, 1 mmol) in 5 mL CH_3OH was mixed into a 5 mL solution of 4-NH_2py (0.1882 g, 2 mmol) and stirred continuously for 2 h. Then, KSCN (0.1944 g, 2 mmol) was added slowly. Heating under reflux and stirring was continued for up to 4 h. The needle-shaped crystals were obtained after several days. Yield: 76.30%, melting point: 220–223 °C.

Synthesis of complex $[ZnCl_2(4\text{-}NH_2py)_2]$

A $[ZnCl_2(4\text{-}NH_2py)_2]$ was synthesized according to a previous report [10]. A $ZnCl_2$ (0.1363 g, 1 mmol) that had been dissolved in 5 mL CH_3OH was mixed with 4-NH_2py (0.1882 g, 2 mmol). The mixture was heated at 64 °C under reflux for 6 h while being continuously stirred. The final solution was chilled to room temperature. Colorless crystals were formed after several days. Yield: 61.23%, melting point: 245–248 °C.

Synthesis of complex $[ZnCl(NCS)(4\text{-}NH_2py)_2]$

A $ZnCl_2$ (0.1363 g, 1 mmol) in 5 mL CH_3OH was mixed into 5 mL solution of 4-NH_2py (0.1882 g, 2 mmol) and stirred continuously for 2 h. Then, KSCN (0.0927 g, 1 mmol) was added slowly. Heating under reflux and stirring was continued for up to 4 h. After a week, colorless crystals were obtained. Yield: 53.79%, melting point: 214–215 °C.

Characterization technique

Melting point temperature was measured in the range of 30–300 °C using a Fisher-John melting point apparatus. The electrical conductivity of complex solutions was measured using Cyberscan CON 11/110 conductivity meter. The infrared spectra were recorded using Shimadzu spectrophotometer type IRPrestige21 on KBr pellets in the range 4000–400 cm^{-1}.

Single crystal X-ray structure determination

Intensity data were gathered at 123 K using Bruker SMART APEX2 diffractometer equipped with a CCD area detector and Mo Kα source (λ = 0.71073 Å)

monochromated by layered confocal mirrors. Data reduction and scaling were performed using Bruker APEX3 suite, and absorption correction was performed using SADABS. SHELXT was used to solve the initial structure, revealing non-hydrogen atoms' positions, which were refined using the SHELXL program on a ShelXle user interface. Anisotropic refinement was performed on non-hydrogen atoms. Hydrogen atoms were placed in the calculated positions using a riding model.

Antibacterial tests

The antibacterial tests were conducted in the Laboratory of Microbiology, Universitas Negeri Malang. The tests were done on different types of pathogen bacteria, gram-positive- *S. aureus* and gram-negative- *E. coli*. The reference antibacterial drug chloramphenicol was evaluated for its antibacterial activity, and the results were compared with those of the free ligands and the complexes. Samples were dissolved in the DMSO 10% to obtain a 5 mg/mL solution. The method used is the disc diffusion method [13,16]. The disc containing antimicrobial agents or compounds was applied to the MHA plate within 20 min after inoculating it with the bacteria. Three discs were coated per petri dish. The plates were inverted and incubated at 37 °C for 24 h. After that, the zones of complete inhibition were measured.

■ RESULTS AND DISCUSSION

Synthesis of Complexes $[Zn(NCS)_2(4\text{-}NH_2py)_2]$ (1), $[ZnCl_2(4\text{-}NH_2py)_2]$ (2), $[ZnCl(NCS)(4\text{-}NH_2py)_2]$ (3)

Three complexes **1**, **2**, and **3** were reacted directly in CH_3OH as a solvent with the mol ratio Zn(II): 4-NH_2py: KSCN of 1:2:0 (complex **1**), 1:2:1 (complex **2**), and 1:2:2 (complex **3**). The results gave colorless crystals with several shapes like needle and beam-shaped, as shown in Fig. 1. The reaction of complex formation is presented in Fig. 2. The reaction of $ZnCl_2$ with 4-NH_2py produced complex $[ZnCl_2(4\text{-}NH_2py)_2]$, then the addition of NCS^- ion substituted the Cl^- ligand to form complexes $[ZnCl(NCS)(4\text{-}NH_2py)_2]$ and $[Zn(NCS)_2(4\text{-}NH_2py)_2]$. Based on the spectrochemical series (Fajans-Tsuchida), the NCS^- ion is stronger than the chloride anion ligand; thus NCS^- can replace Cl^- ligand to form complexes **1** and **3** [24].

Physical Properties of Zinc(II) Complexes 1, 2, 3

All complexes **1**, **2**, and **3** were obtained as colorless crystals (Fig. 1). Complex **1** is needle-shaped crystal (Fig. 1(a)), while complexes **2** (Fig. 1(b)), and **3** (Fig. 1(c)) were block-shaped crystals. The three complexes are air-stable and have sharp melting points around > 200 °C. The melting point data of the three complexes are higher

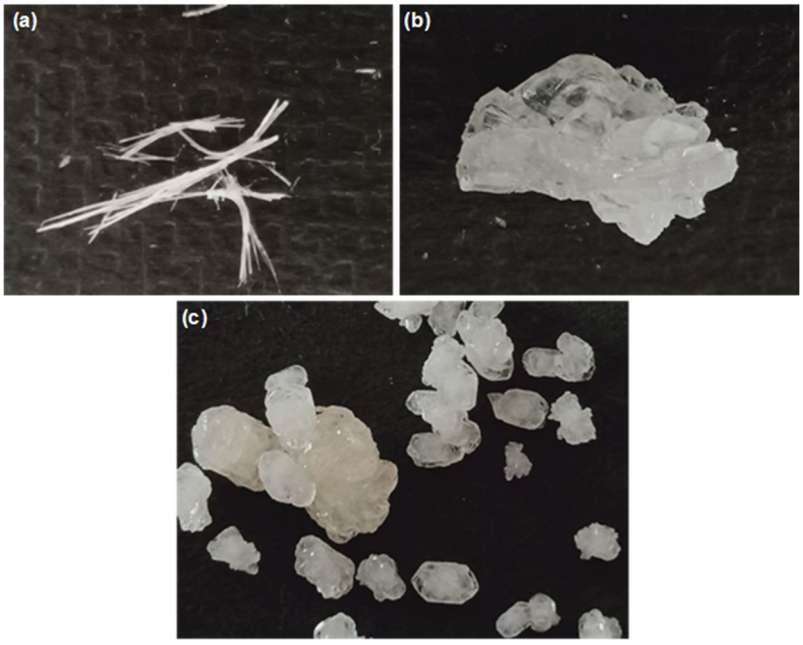

Fig 1. Crystal images of (a) $[Zn(4\text{-}NH_2py)_2(SCN)_2]$ (**1**); (b) $[ZnCl_2(4\text{-}NH_2py)_2]$ (**2**); (c) $[ZnCl(NCS)(4\text{-}NH_2py)_2]$ (**3**)

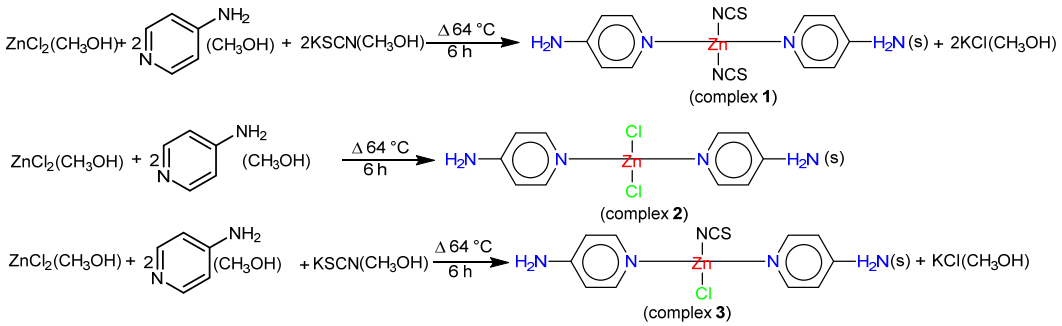

Fig 2. Reaction of the formation Zn(II) complexes **1**, **2**, and **3**

than complex $[Zn(NCS)_2(2\text{-}NH_2py)_2]$ [10] and $[Co(NCS)_2(2\text{-}NH_2py)_2]$ [25]. This could be due to the stronger intermolecular interactions of complexes **1**, **2**, and **3** compared to the two complexes. All complex solutions have been measured for their electrical conductivity in 1 mg/mL using CH_3OH solvent and showed the results: 101.5 µS (complex **1**), 96.3 µS (complex B2), 54.7 µS (complex **3**). These results show that complex solutions are non-electrolytes [26].

Structural Determination of Complexes 1, 2, 3

The reaction between $ZnCl_2$, KSCN, and 4-NH_2py leading to the formation of complexes $[Zn(NCS)_2(4\text{-}NH_2py)_2]$ (**1**), $[ZnCl_2(4\text{-}NH_2py)_2]$ (**2**), and $[ZnCl(NCS)(4\text{-}NH_2py)_2]$ (**3**). The structural determination of all complexes was carried out using single-crystal XRD. The crystallographic data of complexes are shown in Table 1.

Table 1. Crystallographic data

Compound	1	2	3
No. CCDC	2224923	2224925	2224924
Empirical formula	$C_{12}H_{12}N_6S_2Zn$	$C_{10}H_{12}Cl_2N_4Zn$	$C_{11}H_{12}ClN_5SZn$
Empirical mass	369.79	324.53	347.16
System	Orthorombic	Monoclinic	Orthorombic
Space group	Pmmn	C2/c	Pbca
a (Å)	12.9473	8.8309(7)	10.2571(11)
b (Å)	14.3833	9.8240(7)	16.1744(17)
c (Å)	4.1770(8)	14.9961(11)	17.2842(18)
α (°)	90	90	90
β (°)	90	102.3360(10)	90
γ (°)	90	90	90
V (Å^3)	777.827	1268.40(16)	2867.5(5)
Z	2	4	8
T (K)	123	123	123
λ Mo Kα (Å)	0.71073	0.71073	0.71073
F_{000}	376	656	1408
μ (mm^{-1})	1.848	2.339	2.037
D_{calc} (mg/m^3)	1.579	1.699	1.608
θ_{min} (°)	2.116	3.143	2.357
θ_{max} (°)	27.472	27.495	27.574
Goodness of fit	1.129	1.092	1.051
R1 (1 > 2σ(I))	0.0188	0.0209	0.0258
wR2	0.0492	0.0554	0.0611

The structure of complex molecules is shown in Fig. 3. According to Fig. 3, the central ion of all complexes is bonded with two N atoms from two 4-NH_2py molecules and two anions as the ligands to form distorted tetrahedral geometry [8,27-29]. While the bond length of Zn–N pyridine in all complexes has a similar bond length, the angle between N–Zn–N has different distortion depending on ligands [30] (Fig. 4). The bond length of Zn–N2 (2.104 Å) is longer than that of Zn–N1 (1.970 Å) due to the different size of the two ligands. A 4-NH_2py ligand is larger than the NCS^-, and the larger molecular size causes a stronger steric effect; as a result, the distance between Zn and 4-NH_2py is farther apart to reduce the repulsion effect. The steric effect of the ligand also affects the angle of N2–Zn–$N2^i$, which is larger than that of N1–Zn–$N1^i$. The angle between N1–Zn–N2 is smaller than the N2–Zn–$N2^i$ bond angle because the position of 4-NH_2py gives minimal repulsion. Complex **1** also shows a larger N2–Zn–N2 angle distortion compared to complexes **2** and **3**. This may be due to the electronegativity of the N atom of NCS^- (X N = 3.06) being higher than Cl^- (X = 3.16) [31]; the more electronegative the atom, the more it will pull, the more electron density to itself. This decreases the electron pair repulsion between bonded electron pairs on the central atom. Cl^- ligand will pull the bonded electron pair towards itself and away from the central atom. Bond angles between the groups should be reduced when the core atom's electron pair repulsion decreases, so the bond angle between Cl–Zn–Cl will decrease. In addition, the Zn–NCS bonds lengths are shorter compared to Zn–Cl, shorter bond length permits electron-density to be displaced towards zinc to a smaller extent than in Zn–Cl, thus more electron density remains and electron repulsion between the bonded pairs in complex **1** increases and bond angles of complex **1** increases compared to that complex **2** and **3**.

Complex **2** shows that the Zn–Cl bond is longer than that for Zn–N1 (Table 2). This is related to the covalent radius of Cl, which is much longer than the covalent radius N. The angle formed between N1–Zn–N1 and Cl1–Zn–Cl1 in the complex is also smaller than the angle in complex **1**. This is related to the more electronegative of Cl^- ions. The Cl atom will attract the

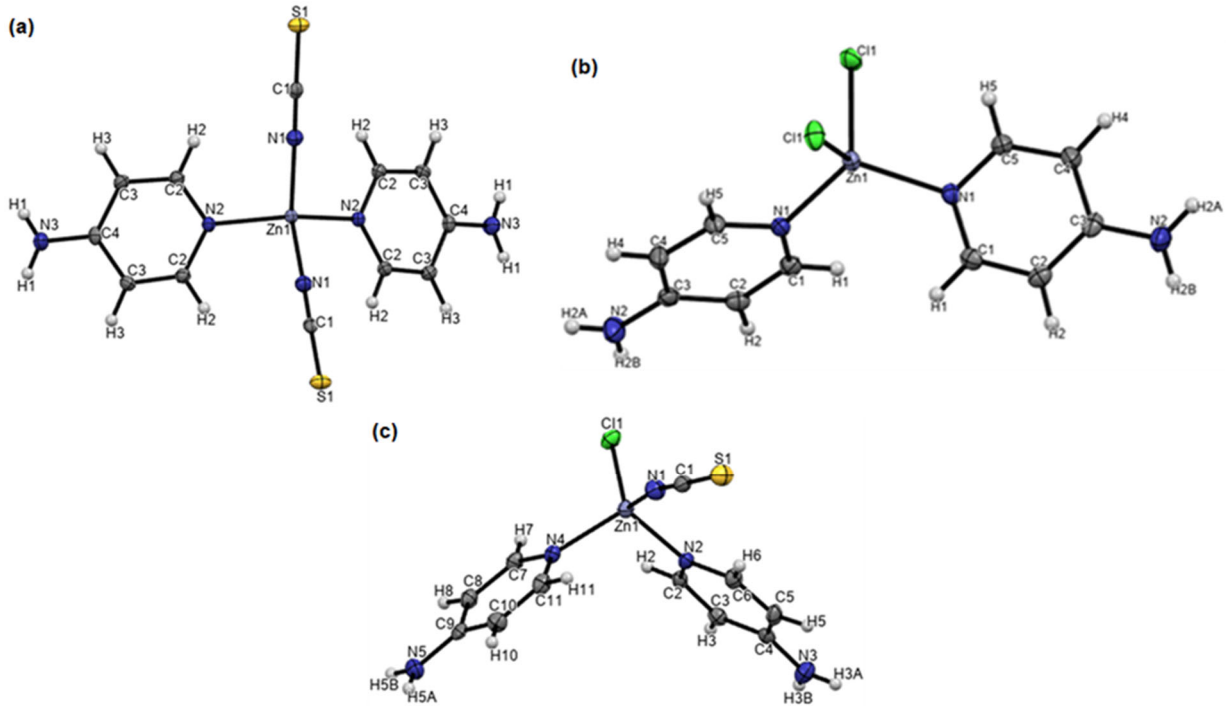

Fig 3. ORTEP view of the structures of (a) [$Zn(NCS)_2(4\text{-}NH_2py)_2$] (**1**); (b) [$ZnCl_2(4\text{-}NH_2py)_2$] (**2**); (c) [$ZnCl(NCS)(4\text{-}NH_2py)_2$] (**3**), showing the atom-labelling scheme. Displacement ellipsoids are drawn at the 50% probability level

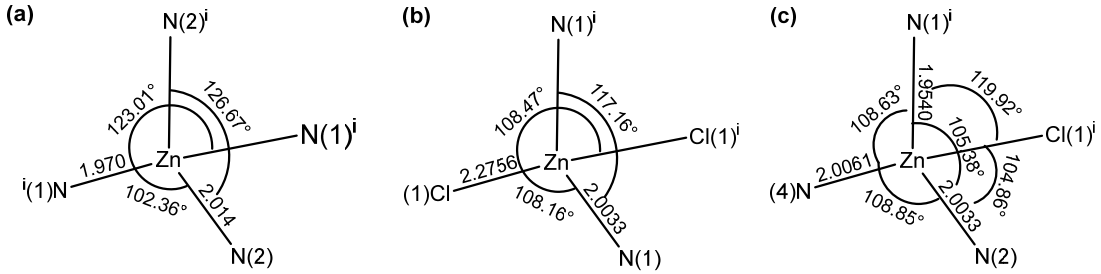

Fig 4. Chemical structures of complexes (a) $[Zn(NCS)_2(4\text{-}NH_2py)_2]$ (**1**); (b) $[ZnCl_2(4\text{-}NH_2py)_2]$ (**2**); (c) $[ZnCl(NCS)(4\text{-}NH_2py)_2]$ (**3**)

Table 2. Selected bond lengths (Å) and angles (°) of **1**–**3**

Complex **1**			
Zn1–N1^i	1.9698(16)	N1^i–Zn1–N1	123.01(10)
Zn1–N1	1.9698(16)	N1^i–Zn1–N2^i	102.36(3)
Zn1–N2^i	2.0140(15)	N1–Zn1–N2^i	102.36(3)
Zn1–N2	2.0141(15)	N1^i–Zn1–N2	102.36(3)
		N1–Zn1–N2	102.36(3)
		N2^i–Zn1–N2	126.67(9)
Complex **2**			
Zn1–N1	2.0033(13)	N1–Zn1–N1^i	117.61(7)
Zn1–N1^i	2.0033(13)	N1–Zn1–Cl1	107.09(4)
Zn1–Cl1	2.2756(4)	N1^i–Zn1–Cl1	108.16(4)
Zn1–Cl1^i	2.2756(4)	N1–Zn1–Cl1^i	108.16(4)
		N1^i–Zn1–Cl1^i	107.09(4)
		Cl1–Zn1–Cl1^i	108.47(2)
Complex **3**			
Zn1–N1	1.9540(16)	N1–Zn1–N4	108.63(7)
Zn1–N4	2.0061(15)	N1–Zn1–N2	105.38(6)
Zn1–N2	2.0192(15)	N4–Zn1–N2	108.85(6)
Zn1–Cl1	2.2575(5)	N1–Zn1–Cl1	119.92(5)
		N4–Zn1–Cl1	108.72(4)
		N2–Zn1–Cl1	104.86 (5)

bonding electrons in its own direction, thereby reducing the bonding electron repulsion on the central atom. In addition, the presence of lone pair electrons in the Cl ligand also reduces the angle of Cl1–Zn–Cl1, N1–Zn–N1, and N1–Zn–Cl1 in complex **2**. This is because the high electrical charge of lone pair electrons causes a strong repulsion, the bond becomes longer, and the angle becomes smaller.

The three complexes have the same geometry; however, they crystallize in different space groups. Complex **1** is isostructural with $[Co(NCS)_2(4\text{-}NH_2py)_2]$ [27], it crystallizes in an orthorhombic space group Pmmn, and there are complex **2** molecules of $[Zn(NCS)_2(4\text{-}NH_2py)_2]$ in 1 unit cell (Fig. 5(a)). The Zn(II) ion in complex **1** is in the special mm2 position, and the asymmetric unit only contains a quarter of the molecule. Weak interaction was also observed between the H from the NH_2 group and the S of SCN (N-H···S-CN) (2.715 Å). Complex **2** showed an isostructural result with complex $[CoCl_2(4\text{-}NH_2py)_2]$ that was reported by Sanchez Montilva et al. [12]. Complex from $ZnCl_2$ and 4-NH_2py have been synthesized by Moustafa et al. [4], but the obtained complex had a different structure from the complex we reported. As-synthesized complex **2** crystallizes in monoclinic with the C2/c space group and 4 complex molecules in each unit cell (see Fig. 5(b)). The central atom is located on 2 folding axes, and the asymmetric unit only contains half of the molecule. Non-covalent interactions such as N-H···Cl (2.8336 Å) and weak μ···μ stacking interactions between C atoms of two 4-NH_2py (C4···C5 3.371 Å) and (C4···C4 3.172 Å) are observed in complex **2**. The non-covalent interaction of N-H···Cl enables the formation of unlimited chains through the ac plane. Meanwhile, asymmetric complex **3** crystallizes in the Pbca group with 8 molecules in each unit cell (see Fig. 5(c)). Weak interaction between Cl···H-NH (2.554 Å) and S···H-NH (2.843 Å) are also observed in the packing crystal system of complex **3**.

FTIR Spectroscopy

Although it is commonly accepted that for N-bound thiocyanate complexes, ν_{SC} exhibits higher frequency values and ν_{CN} shows lower frequency values, these principles must be applied with caution because a variety of other factors can affect the locations of these bands.

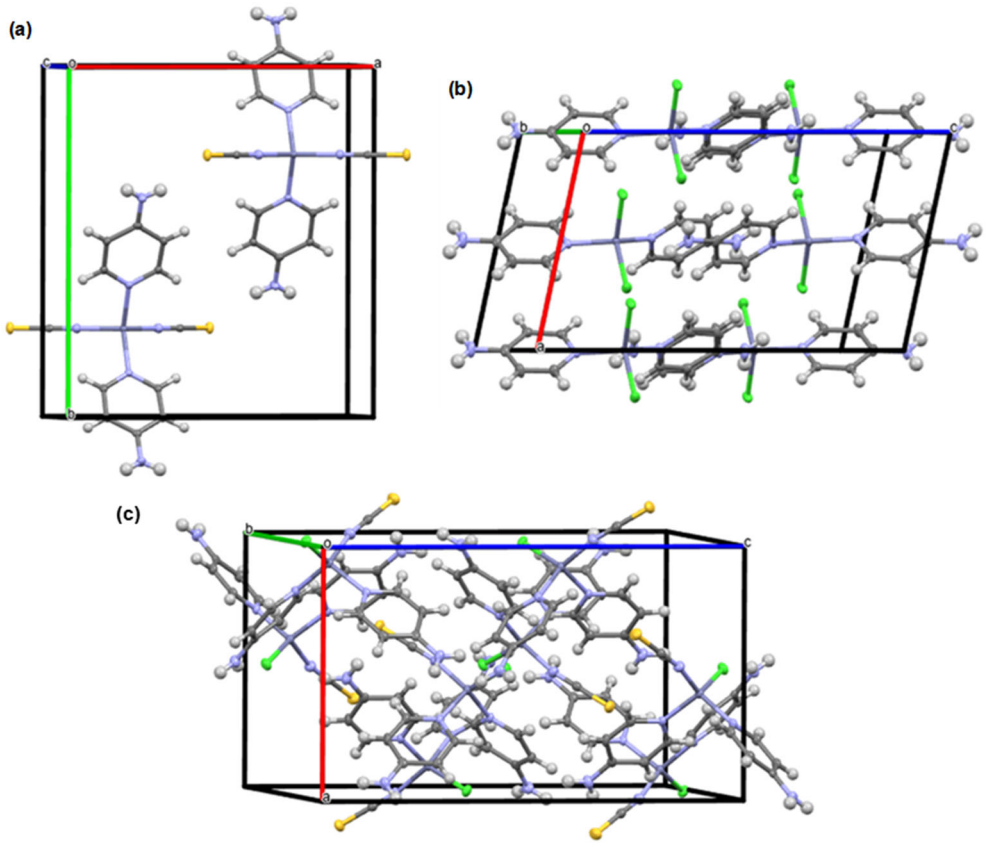

Fig 5. Packing diagrams of (a) $[Zn(NCS)_2(4\text{-}NH_2py)_2]$ (**1**); (b) $[ZnCl_2(4\text{-}NH_2py)_2]$ (**2**); (c) $[ZnCl(NCS)(4\text{-}NH_2py)_2]$ (**3**)

Table 3. Selected wavenumbers (cm^{-1}) of ligands in the tree complexes

Assignment	4-NH_2py	KSCN	**1**	**2**	**3**
$\nu_{as}(NH_2)$	3439s		3443s	3443s	3470s
$\nu_s(NH_2)$	3305s		3341s	3341s	3346s
ν_{ring}	1682s,		1655s,	1659s,	1643s,
	1584s, 1337s		1633s,	1634s,	1634s,
			1362m	1352s	1352s
ν(C-NH_2)	1217s		1219s	1223s	1211s
ν_{CN}		2170s	2056m		2050m
ν_{SC}		743s	817s		829s

We already know, based on the crystal structure, that all metal ions of complexes **1**-**3** are bonded to the thiocyanate ions through the N atom. This is also proved by the appearance of ν_{CN} bands around 2050 cm^{-1} (Table 3) [2,32]. The ν_{SC} in complexes **1** and **3** were observed around 820–850 cm^{-1}. These bands are in accordance with N–bonding behavior (ν_{SC} 760–860 cm^{-1}) compared to S–bonding behavior (ν_{SC} 690–720 cm^{-1}) (Fig. 6). Meanwhile, according to structure crystals data, it appears that 4-NH_2py ligands bind to the Zn(II) ions through the nitrogen atom of the pyridine ring. The $\nu(NH_2)$ (symmetric and asymmetric) bands do not show a significant shift in wavenumber (see Table 3), and it is generally known that the NH_2 stretching vibrations undergo a significant red shift when $-NH_2$ in 2-aminopyridine forms a coordination bond with metal ions (Δ = 150–200 cm^{-1}) [33]. Therefore, it is proved that the NH_2 group is not directly involved in the formation of coordination bonds.

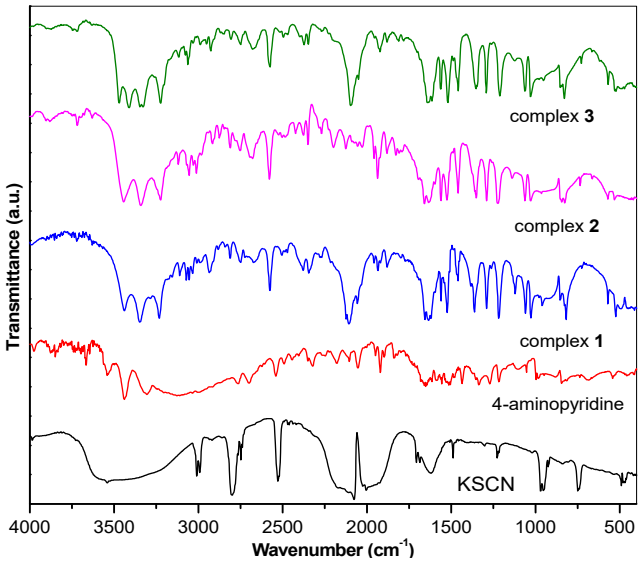

Fig 6. FTIR spectra of complexes and ligands

Antibacterial Activity

Fig. 7 and 8 show the results of the antibacterial test of complexes **1**, **2** and **3** against *E. coli* and *S. aureus*. The test results in the form of the diameter of the inhibition zones (mm) are presented in Table 4. Fig. 4 and 5 show that complexes **1** and **2** give a better antibacterial activity than their metal salt and free ligands. We observed that the antibacterial activity of complexes and 4-NH_2py is through the formation of hydrogen bonds between the cell membrane and N atom from 4-NH_2py and blocking the way for nutrients to enter the cell [17]. The antibacterial activity of complexes increase in order [Zn(4-NH_2py)$_2$Cl$_2$] (**2**) < [Zn(4-NH_2py)$_2$(NCS)Cl] (**3**) < [Zn(4-NH_2py)$_2$(NCS)$_2$] (**1**). This indicates that co-ligands also play an important role in increasing their antimicrobial activity. Complexes with thiocyanate exhibit better antibacterial activity than that with chloride ions. The

Table 4. Diameter of inhibition zones of the ligands, metal salt and complexes

Compounds	Inhibition zones (mm)	
	S. aureus	*E. coli*
4-NH_2py	6.7	6.3
KSCN	10.0	6.7
$ZnCl_2$	7.5	11.9
[Zn(4-NH_2py)$_2$(NCS)$_2$] (**1**)	11.6	12.1
[Zn(4-NH_2py)$_2$Cl$_2$] (**2**)	6.8	6.0
[Zn(4-NH_2py)$_2$(NCS)Cl] (**3**)	11.1	10.8
Chloramphenicol	31.5	34.0

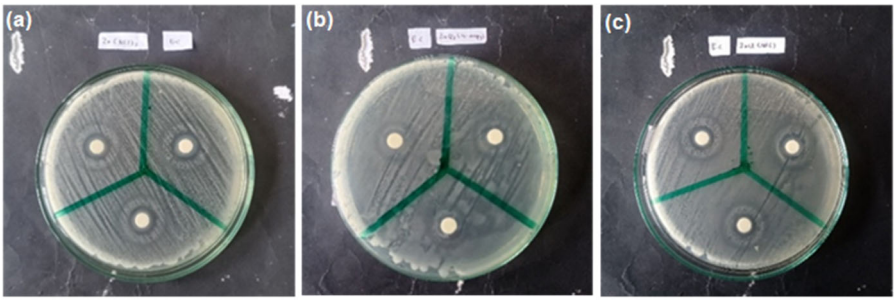

Fig 7. Zone inhibition against *E. coli* with complexes (a) **1**; (b) **2**, and (c) **3**

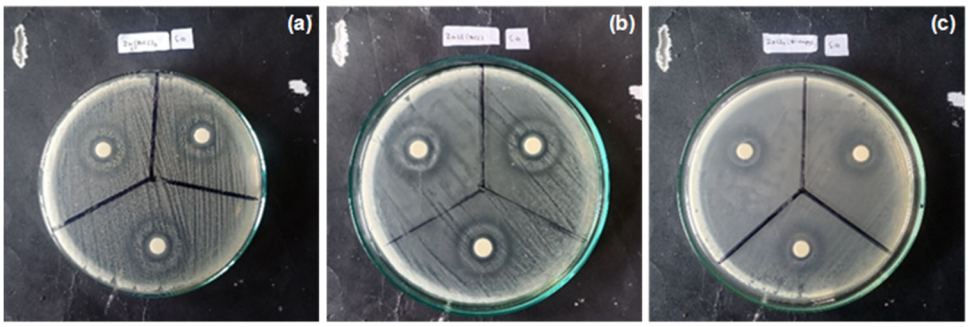

Fig 8. Zone inhibition against *S. aureus* with complexes (a) **1**; (b) **2**, and (c) **3**

antibacterial activity of a complex is affected by its structure and stability, acid-base properties, donor atoms, lipophilicity and the most preferred binding site for biomolecules [34]. We hypothesize that increasing antibacterial activity in these complexes was influenced by several factors. First, based on the spectrochemical series (Fajans-Tsuchida), NCS^- is a stronger ligand than Cl^- [31], leading to the interaction NCS^- with Zn(II) is stronger than Zn(II) and Cl^-. This interaction will decrease the polarity of the metal ion due to the partial sharing of positive charge with the donor atom, resulting in the delocalization of electrons within metal complexes [3,16,25]. This may increase the lipophilic character of the metal complex, thus allowing it to penetrate the lipid layer of the bacterial membrane more easily [3,16,25]. Secondly, the slow release of Zn(II) in bacteria cells could lead to an interaction formation of the metal ion with nucleic acids and deactivate the enzymes of the respiratory system [35]. Lastly, the substituent group, such as $-NH_2$ interacts with a polar site of bacteria cell wall and disrupt the passage of solutes between the cell and the outer environment [36-39]; the metal ions also could bind to SH (sulfhydryl group) of the cell enzyme and breakdown the cell membrane [40]. Several other complexes, such as $[Zn(NCS)_2(2\text{-}NH_2py)_2]$ [10], $[Co(L)_2(2\text{-}NH_2py)_2]$ (L = $[N(CN)_2]$, NCS^-) [3,25], have been reported to exhibit a low to moderate antibacterial activity. The complex **1** has similar inhibition zones with $[Zn(NCS)_2(2\text{-}NH_2py)_2]$ [10] around 11 mm, while $[Co(L)_2(2\text{-}NH_2py)_2]$ (L = $[N(CN)_2]$, NCS^-) [3,25], and $[Mn(dca)_2(2\text{-}NH_2py)_2]$ [7] have higher antibacterial activity than the three complexes.

■ CONCLUSION

Three complexes $[Zn(4\text{-}NH_2py)_2(NCS)_2]$ **1**, $[Zn(4\text{-}NH_2py)_2Cl_2]$ **2**, and $[Zn(4\text{-}NH_2py)_2(NCS)Cl]$ **3** have been successfully synthesized, and the yields obtained were 76.30%, 61.23%, and 53.79%, respectively. The Zn(II) in all complexes bind two N atoms of two 4-NH_2py rings and 2 anionic ligands to form distorted tetrahedral geometry. The three complexes crystallize in different crystal lattices such as Pmmn (**1**), C2/c (**2**), and Pbca (**3**). Non-covalent interactions between 4-NH_2py and anionic ligands are observed to play a role in the crystal packing of all complexes. The preliminary antimicrobial screening against *S. aureus* and *E. coli* bacteria indicates that the complexes are moderately active. In this study, the complexes with thiocyanate ion exhibit greater antibacterial activity than with chloride ion due to stronger interaction with the central ion that leads to the increasing the lipophilic character of the metal complex.

■ SUPPORTING INFORMATION

Crystallographic data for the structural information have been put on deposit in the Cambridge Crystallographic Data Centre, CCDC no. 2224923-2224925. Copies of this information may be obtained from The Director, CCDC, 12 Union Road, Cambridge, CB2 1EZ, UK (fax: +44-1233-336033; e-mail: deposit@ccdc.cam.ac.uk or www: http://www.ccdc.cam.ac.uk).

■ ACKNOWLEDGMENTS

Universitas Negeri Malang, Indonesia, is gratefully acknowledged for funding this research through Internal funds in 2022 (contract number: 19.5.909/UN32.20.1/LT/2022). We also thank the Department of Applied Chemistry at Hiroshima University for using XRD single crystal.

■ AUTHOR CONTRIBUTIONS

I Wayan Dasna and Dewi Mariyam conducted the experiment. I Wayan Dasna, Husni Wahyu Wijaya and Dewi Mariyam concept the methodology. Sugiarto conducted the structure crystal determination, and I Wayan Dasna, Husni Wahyu Wijaya, Ubed Sonai Fahruddin Arrozi, Sugiarto and Dewi Mariyam wrote and revised the manuscript. All authors agreed to the final version of this manuscript.

■ REFERENCES

[1] Pal, S., 2018, "Pyridine: A Useful Ligand in Transition Metal Complexes" in *Pyridine*, Eds. Pandey, P.P., IntechOpen, Rijeka, Croatia, 57–74.

[2] Handy, J.V., Ayala, G., and Pike, R.D., 2017, Structural comparison of copper(II) thiocyanate pyridine complexes, *Inorg. Chim. Acta*, 456, 64–75.

[3] Yuoh, A.C.B., Agwara, M.O., Yufanyi, D.M., Conde, M.A., Jagan, R., and Oben Eyong, K., 2015, Synthesis, crystal structure, and antimicrobial properties of a novel 1-D cobalt coordination polymer with dicyanamide and 2-aminopyridine, *Int. J. Inorg. Chem.*, 2015, 106838.

[4] Moustafa, M.E., Meshal, N.M., Ayad, M.I., and Goda, O.A., 2020, Aminopyridine transition metals complexes; Characterization, application and molecular orbital calculation, *Benha J. Appl. Sci.*, 5 (7), 231–243.

[5] Mautner, F.A., Jantscher, P., Fischer, R.C., Torvisco, A., Vicente, R., Karsili, T.N.V., and Massoud, S.S., 2019, Synthesis and characterization of 1D coordination polymers of metal(II)-dicyanamido complexes, *Polyhedron*, 166, 36–43.

[6] Suckert, S., Terraschke, H., Reinsch, H., and Näther, C., 2017, Synthesis, crystal structures, thermal, magnetic and luminescence properties of Mn(II) and Cd(II) thiocyanate coordination compounds with 4-(Boc-amino)pyridine as co-ligand, *Inorg. Chim. Acta*, 461, 290–297.

[7] Mbani, A.L.O., Yufanyi, D.M., Tabong, C.D., Hubert, N.J., Yuoh, A.C.B., Paboudam, A.G., and Ondoh, A.M., 2022, Synthesis, crystal structure, DFT studies and Hirshfeld surface analysis of manganese(II) and cadmium(II) coordination polymers of 2-aminopyridine and dicyanamide, *J. Mol. Struct.*, 1261, 132956.

[8] Mautner, F.A., Jantscher, P.V., Fischer, R.C., Torvisco, A., Reichmann, K., and Massoud, S.S., 2021, Syntheses, structural characterization, and thermal behaviour of metal complexes with 3-aminopyridine as co-ligands, *Transition Met. Chem.*, 46 (3), 191–200.

[9] Yufanyi, D.M., Nono, H.J., Yuoh, A.C.B., Tabong, C.D., Judith, W., and Ondoh, A.M., 2021, Crystal packing studies, thermal properties and hirshfeld surface analysis in the Zn(II) complex of 3-aminopyridine with thiocyanate as co-ligand, *Open J. Inorg. Chem.*, 11 (3), 63–84.

[10] Mariyam, D., Farida, N., Wijaya, H.W., and Dasna, I.W., 2022, Studi karakterisasi dan aktivitas antibakteri senyawa kompleks dari zink(II) klorida, kaliumtiosianat dan 2-aminopiridina, *J. Ris. Kim.*, 13 (1), 100–110.

[11] Kartal, Z., and Şahin, O., 2021, The synthesis of heteroleptic cyanometallate aminopyridine complexes and an investigation into their structural properties with various spectroscopic methods, *J. Mol. Struct.*, 1227, 129514.

[12] Sanchez Montilva, O.C., Movilla, F., Rodriguez, M.G., and Di Salvo, F., 2017, Synthesis, crystal structure and study of the crystal packing in the complex bis(4-aminopyridine-κN1)dichloridocobalt(II), *Acta Crystallogr., Sect. C: Struct. Chem.*, 73 (5), 399–406.

[13] Wöhlert, S., Jess, I., Englert, U., and Näther, C., 2013, Synthesis and crystal structures of Zn(II) and Co(II) coordination compounds with *ortho* substituted pyridine ligands: Two structure types and polymorphism in the region of their coexistence, *CrystEngComm*, 15 (26), 5326–5336.

[14] Jochim, A., Radulovic, R., Jess, I., and Näther, C., 2020, Crystal structure of bis(tetramethylthiourea-κS)bis(thiocyanato-κN)cobalt(II), *Acta Crystallogr., Sect. E: Crystallogr. Commun.*, 76 (8), 1373–1377.

[15] Jafari, M., Salehi, M., Kubicki, M., Arab, A., and Khaleghian, A., 2017, DFT studies and antioxidant activity of Schiff base metal complexes of 2-aminopyridine. Crystal structures of cobalt(II) and zinc(II) complexes, *Inorg. Chim. Acta*, 462, 329–335.

[16] Tsague Chimaine, F., Yufanyi, D.M., Colette Benedicta Yuoh, A., Eni, D.B., and Agwara, M.O., 2016, Synthesis, crystal structure, photoluminescent and antimicrobial properties of a thiocyanato-bridged copper(II) coordination polymer, *Cogent Chem.*, 2 (1), 1253905.

[17] Setifi, Z., Geiger, D., Jelsch, C., Maris, T., Glidewell, C., Mirzaei, M., Arefian, M., and Setifi, F., 2018, The first Fe(II) complex bearing end-to-end dicyanamide as a double bridging ligand: Crystallography study and Hirshfeld surface analysis; completed with a CSD survey, *J. Mol. Struct.*, 1173, 697–706.

[18] Nath, R.K., Roy, T.G., and Sutradhar, R.K., 2017, Synthesis of some Cd(II) and Zn(II) complexes of a tetraazamacrocyclic ligand and their antimicrobial activities, *Asian-Australas. J. Biosci. Biotechnol.*, 2 (2), 136–144.

[19] Day, B.J., 2019, The science of licking your wounds: Function of oxidants in the innate immune system, *Biochem. Pharmacol.*, 163, 451–457.

[20] Magacz, M., Kędziora, K., Sapa, J., and Krzyściak, W., 2019, The significance of lactoperoxidase system in oral health: Application and efficacy in oral hygiene products, *Int. J. Mol. Sci.*, 20 (6), 1443.

[21] Prasch, J., Bernhart, E., Reicher, H., Kollroser, M., Rechberger, G.N., Koyani, C.N., Trummer, C., Rech, L., Rainer, P.P., Hammer, A., Malle, E., and Sattler, W., 2020, Myeloperoxidase-derived 2-chlorohexadecanal is generated in mouse heart during endotoxemia and induces modification of distinct cardiomyocyte protein subsets *in vitro*, *Int. J. Mol. Sci.*, 21 (23), 9235.

[22] Mishra, O.P., Popov, A.V., Pietrofesa, R.A., Nakamaru-Ogiso, E., Andrake, M., and Christofidou-Solomidou, M., 2018, Synthetic secoisolariciresinol diglucoside (LGM2605) inhibits myeloperoxidase activity in inflammatory cells, *Biochim. Biophys. Acta, Gen. Subj.*, 1862 (6), 1364–1375.

[23] Li, F., Xiong, X.S., Yang, Y.Y., Wang, J.J., Wang, M.M., Tang, J.W., Liu, Q.H., Wang, L., and Gu, B., 2021, Effects of NaCl concentrations on growth patterns, phenotypes associated with virulence, and energy metabolism in *Escherichia coli* BW25113, *Front. Microbiol.*, 12, 705326.

[24] Effendy, E., 2007, *Perspektif Baru Kimia Koordinasi Jilid 1*, Bayumedia Publishing, Malang.

[25] Munadhiroh, A., Wijaya, H.W., Farida, N., Golhen, S., and Dasna, I.W., 2022, Synthesis, characterization, and preliminary study of [Co(2-aminopyridine)$_2$(NCS)$_2$] or bis(2-aminopyridine)dithiocyanato cobalt(II) as an antibacterial, *J. Kim. Valensi*, 8 (1), 23–29.

[26] Svirchuk, Y.S., 2006, Electrical Conductivity, *A-to-Z Guide to Thermodynamics, Heat & Mass Transfer, and Fluids Engineering*, e (l), 1–13.

[27] Sugiyama, H., Sekine, A., and Uekusa, H., 2015, Crystal structure of bis(4-aminopyridine)bis(isothiocyanato)cobalt(II), *X-Ray Struct. Anal. Online*, 31, 2014–2015.

[28] Makhlouf, J., Valkonen, A., and Smirani, W., 2022, Transition metal precursor impact on thiocyanate complexes crystallization: Isomorphous cobalt and nickel properties, *Polyhedron*, 213, 115625.

[29] Moustafa, I.M.I., Mohamed, N.M., and Ibrahim, S.M., 2022, Molecular modeling and antimicrobial screening studies on some 3-aminopyridine transition metal complexes, *Open J. Inorg. Chem.*, 12 (3), 39–56.

[30] Linker, G.J., van Duijnen, P.T., and Broer, R., 2020, Understanding trends in molecular bond angles, *J. Phys. Chem. A*, 124 (7), 1306–1311.

[31] Effendy, E., 2017, *Molekul, Struktur dan Sifat-Sifatnya*, Indonesian Academic Publishing, Malang, Indonesia.

[32] Nakamoto, K., 2006, "Infrared and Raman Spectra of Inorganic and Coordination Compounds" in *Handbook of Vibrational Spectroscopy*, Eds. Chalmers, J.M., and Griffiths, P.R., Wiley, Hoboken, US.

[33] Buyukmurat, Y., and Akyuz, S., 2003, Theoretical and experimental studies of IR spectra of 4-aminopyridine metal(II) complexes, *J. Mol. Struct.*, 651-653, 533–539.

[34] Ramotowska, S., Wysocka, M., Brzeski, J., Chylewska, A., and Makowski, M., 2020, A comprehensive approach to the analysis of antibiotic-metal complexes, *TrAC, Trends Anal. Chem.*, 123, 115771.

[35] Claudel, M., Schwarte, J.V., and Fromm, K.M., 2020, New antimicrobial strategies based on metal complexes, *Chemistry*, 2 (4), 849–899.

[36] Tevyashova, A.N., and Tevyashova, A.N., 2021, Recent trends in synthesis of chloramphenicol new derivatives, *Antibiotics*, 10 (4), 370.

[37] Dinos, G.P., Athanassopoulos, C.M., Missiri, D.A., Giannopoulou, P.C., Vlachogiannis, I.A., Papadopoulos, G.E., Papaioannou, D., and Kalpaxis, D.L., 2016, Chloramphenicol derivatives

as antibacterial and anticancer agents: Historic problems and current solutions, *Antibiotics*, 5 (2), 20.

[38] Tsirogianni, A., Kournoutou, G.G., Bougas, A., Poulou-Sidiropoulou, E., Dinos, G., and Athanassopoulos, C.M., 2021, New chloramphenicol derivatives with a modified dichloroacetyl tail as potential antimicrobial agents, *Antibiotics*, 10 (4), 394.

[39] Kostopoulou, O.N., Magoulas, G.E., Papadopoulos, G.E., Mouzaki, A., Dinos, G.P., Papaioannou, D., and Kalpaxis, D.L., 2015, Synthesis and evaluation of chloramphenicol homodimers: Molecular target, antimicrobial activity, and toxicity against human cells, *PLoS One*, 10 (8), e0134526.

[40] Al–Shaheen, A.J., 2010, Study on synthesis and antibacterial activity of Co(II) and Ni(II) complexes including isopropylacetone thiosemicarbozone and cresol, *Iraqi Natl. J. Chem.*, 37, 111–127.